# Hybrid LMS-MMSE Inverse Halftoning Technique

Pao-Chi Chang, Che-Sheng Yu, and Tien-Hsu Lee

***Abstract*—The objective of this work is to reconstruct high quality gray-level images from bilevel halftone images. We develop optimal inverse halftoning methods for several commonly used halftone techniques, which include dispersed-dot ordered dither, clustered-dot ordered dither, and error diffusion. At first, the least-mean-square (LMS) adaptive filtering algorithm is applied in the training of inverse halftone filters. The resultant optimal mask shapes are significantly different for various halftone techniques, and these mask shapes are also quite different from the square shape that was frequently used in the literature. In the next step, we further reduce the computational complexity by using lookup tables designed by the minimum mean square error (MMSE) method. The optimal masks obtained from the LMS method are used as the default filter masks. Finally, we propose the hybrid LMS-MMSE inverse halftone algorithm. It normally uses the MMSE table lookup method for its fast speed. When an empty cell is referred, the LMS method is used to reconstruct the gray-level value. Consequently, the hybrid method has the advantages of both excellent reconstructed quality and fast speed. In the experiments, the error diffusion yields the best reconstruction quality among all three halftone techniques.**

***Index Terms*—Error diffusion, inverse halftoning, LMS adaptive filter, MMSE table lookup, ordered dithering.**

## I. Introduction

HALFTONE techniques, which convert gray-level images into bilevel images, have been widely applied to the printing of newspapers, magazines, books, as well as fax machines and printers [1], [2]. The inverse halftoning processes, i.e., the reconstruction of gray-level images from bilevel halftoned images, also get increasing attention. The reconstruction process is necessary in at least two situations. The first is when the output device is capable of showing color or gray-level images, such as the computer display, a carefully reconstructed continuous-tone image should deliver better quality than a halftone image for an original continuous-tone image. The second is when an image processing technique is applied to a halftone image, it will be more accurate to process it in the original continuous-tone domain [3]. Moreover, halftoning is basically a lossy process. It is impossible to get a perfect reconstruction without distortion from a halftone image. Nevertheless, it is interesting to know how close the reconstruction quality can be to the original image.

In this work, we discuss inverse halftoning techniques for the three most widely used halftone techniques, which include dispersed-dot ordered dither, clustered-dot ordered dither, and error diffusion [1]. We consider a general inverse halftoning process that includes two parts, the classification and the reconstruction. Halftone classification is the pre-processing of reconstruction. Different halftone techniques result in very different statistical properties. A successful classification can allow a distinct design of reconstruction filters with respect to each halftone technique, consequently yield better reconstruction quality. We have previously presented a classification technique with back propagation neural networks based on the enhanced one- dimensional correlation of halftone images [4]. It can correctly classify several most widely used halftoning techniques. Thus in this paper, we assume that the applied halftoning method can be determined from the halftone images, and we are able to design different reconstruction filters for different halftone methods.

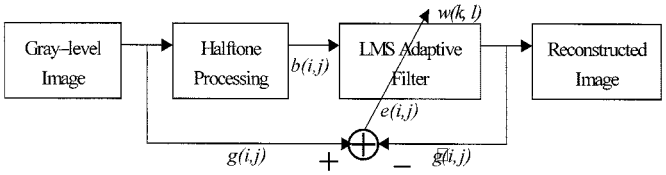


Fig. 1. Block diagram of the LMS adaptive filtering algorithm in the training of inverse halftone reconstruction.

The objective of inverse halftone reconstruction is to convert halftoned bilevel images into gray-level images with the minimum distortion. The performance of halftone reconstruction is measured by PSNR, i.e., the peak signal power to the mean squared error (MSE) between the original gray-level and the reconstructed gray-level images. There exist several inverse halftoning techniques, including iterative projection [5]–[9], neural network [10], vector quantization [11], table lookup [3], wavelet [12], linear and/or nonlinear filtering [13]–[17], and MAP estimation [18], [19]. Most of these techniques yield good reconstruction image quality but need iterative computations, which require relatively high computational complexity. Therefore, we focus on the development of inverse halftoning techniques with excellent performance and affordable complexity for practical use.

Normally, the reconstruction process is a sliding window filtering process. The major parameters are the filter order, i.e., the number of pixels used, the filter shape, i.e. the mask, and the filter coefficients, i.e., weights. It is not obvious to design optimal reconstruction filters for various halftone techniques. In this situation, the adaptive filtering which adjusts the weights based on the statistics of the original gray-level image and the filter output image is a very good approach [20]. We choose the LMS algorithm for its low complexity and excellent performance. Kim *et al.*, applied the LMS algorithm to binary permutation filters for inverse halftoning [6]. Chen and Hang used the

Manuscript received December 8, 1998; revised July 21, 2000. This work was supported by Chung-Hua Telecom. Laboratories, Taiwan, R.O.C., under Grant TL 86–5205. The associate editor coordinating the review of this manuscript and approving it for publication was Prof. Jan P. Allebach.

The authors are with the Department of Electrical Engineering, National Central University, Chung-Li, Taiwan 320, R.O.C. (e-mail: pcchang@ee.ncu.edu.tw).

Publisher Item Identifier S 1057-7149(01)00106-3.

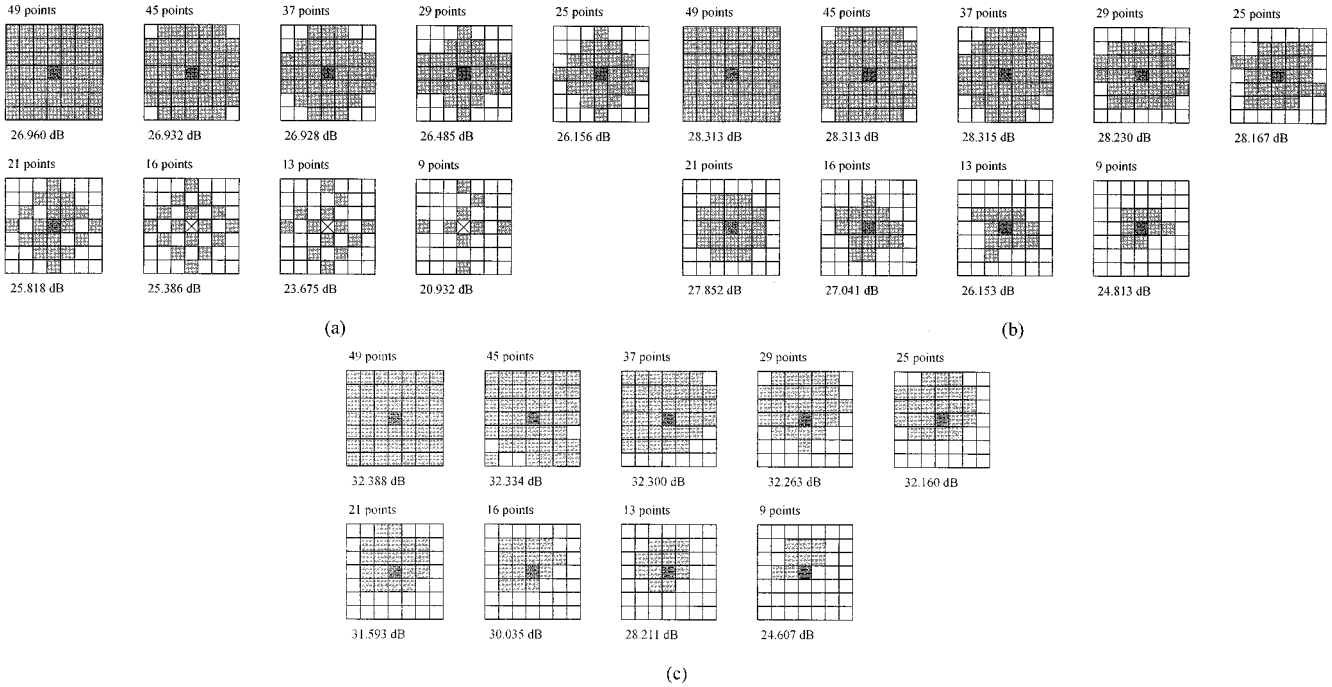


Fig. 2. Variations of the LMS filter mask shapes and the PSNR values (dB) of the reconstructed image *Lena*: (a) clustered-dot ordered dither, (b) dispersed-dot ordered dither, and (c) error diffusion.

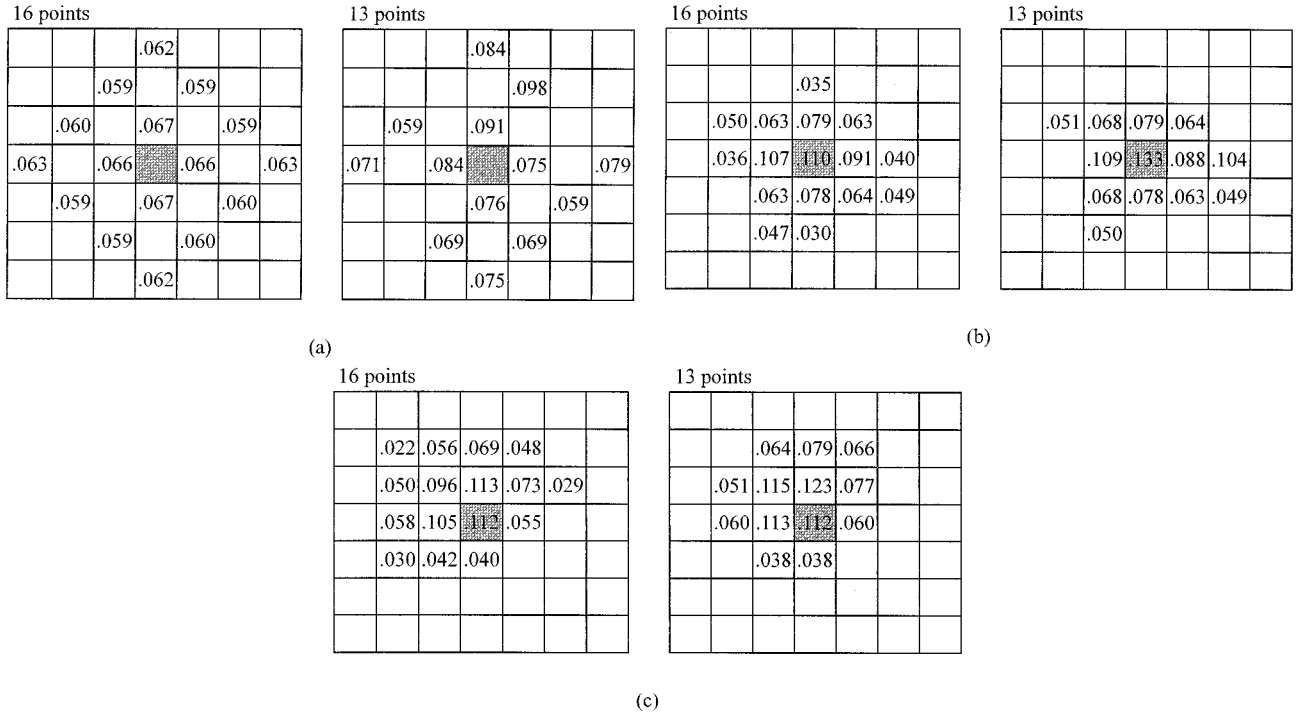


Fig. 3. Coefficients of the 16-point and 13-point filters designed by the LMS method: (a) clustered-dot ordered dither, (b) dispersed-dot ordered dither, and (c) error diffusion.

LMS to design filters with the default square shape and developed an adaptive postprocessing algorithm [21]. In this work, we do not assume a default filter mask shape at the beginning. Instead, we apply the LMS algorithm to determine optimal mask shapes and weights for various halftone techniques.

Practically, the inverse halftoning reconstruction filters can be implemented by table lookup with reasonably large table sizes since the input images are bilevel. One way to build the table is to use the results designed by the LMS algorithm since it is optimal provided that the input images are stationary and ergodic. However, the LMS algorithm may track to the local statistics if the training image set is not sufficiently large or the updating step size is not carefully tuned. Therefore, we present a different approach to the design of reconstruction tables. The halftoning and inverse

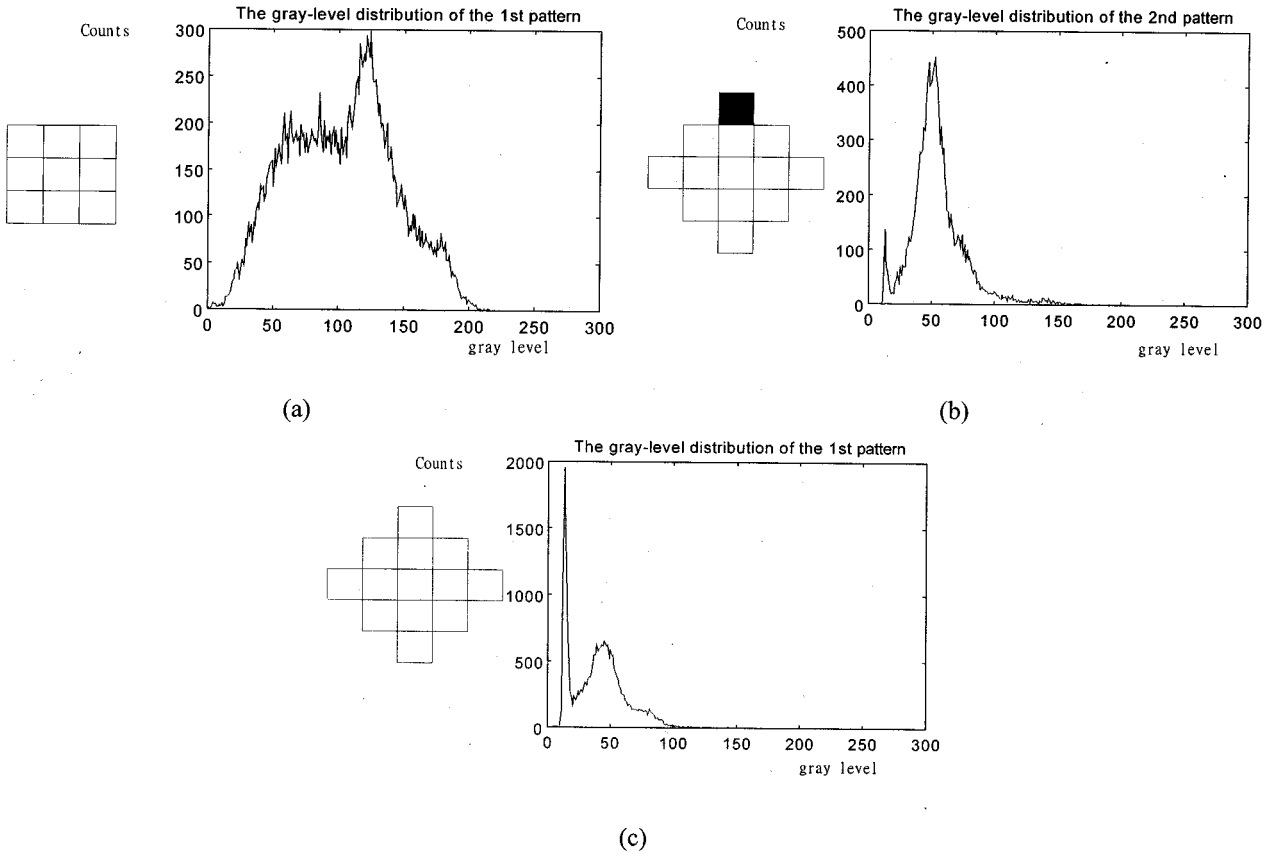


Fig. 4. Halftone patterns and the corresponding histograms of the grey-level distribution for the central pixel in clustered-dot ordered dither: (a) 9-point mask, (b) 13-point mask, and (c) 13-point mask.

halftoning processes can be interpreted as the encoding and decoding processes of vector quantization. Therefore, the codebook design methods can be applied to build the inverse halftoning lookup tables [22]. The content of a table entry is the centroid of the input samples that are mapped to this entry. The results are optimal in the sense of minimizing the MSE for a given halftone method.

Although the MMSE table lookup method has the advantages of good reconstructed quality and fast speed, it faces the *empty cell* problem in which no or very few training samples are mapped to a specific halftone pattern. Hence, we propose a hybrid scheme that combines the above two methods. Normally, the MMSE table lookup method is the first choice. The LMS method is used if an empty cell is encountered in the table lookup process. Consequently, this hybrid method yields the best performance.

This paper is organized as follows. In Section II we describe the inverse halftone reconstruction by LMS adaptive filtering technique. The inverse halftone reconstruction by the MMSE table lookup method is presented in Section III. The hybrid LMS-MMSE algorithm is proposed in Section IV. Finally, conclusions are given in Section V.

## II. Inverse Halftoning by LMS Adaptive Filtering

### A. Adaptation Algorithm

An adaptive filter is basically a self-adjustable digital filter that includes two major parts, the filter itself, and the adaptive algorithm used to adjust the filter weights [20]. In this work, the inverse halftoning filter is designed by the adaptive algorithm. The whole process includes two phases, training and on-line reconstruction. The weight adaptation is only applied to the training in which both the original and the halftone images are available.

The structure of the training process for inverse halftone reconstruction is shown in Fig. 1. The reconstructed image is generated by a sliding linear filter over the binary image, as computed by

$$\widehat{g}(i, j) = \sum_{(k,l)\in M} w(k, l)b(i-k, j-l) \tag{1}$$

where

| | |
|---|---|
| $\widehat{g}(i, j)$ | reconstructed gray-level pixel located at $(i, j)$; |
| $w(k, l)$ | filter weight; |
| $M$ | filter mask which is a set of pixels centered around $(i, j)$; |
| $b(i-k, j-l)$ | bilevel halftoned pixel at the location $(i-k, j-l)$. |

The goal of the filter adaptation is toward to the minimization of the MSE. The reconstruction error $e(i, j)$ is defined as the difference between the original gray-level pixel $g(i, j)$ and the reconstructed gray-level pixel $\widehat{g}(i, j)$, i.e.,

$$e(i, j) = g(i, j) - \widehat{g}(i, j). \tag{2}$$

TABLE I
PSNR (dB) OF THE RECONSTRUCTED IMAGES WITH VARIOUS MASK SIZES AND HALFTONE METHODS

| Image | Method \ Mask Size | | 9 | 13 | 16 | 21 | 25 | 49 |
|---|---|---|---|---|---|---|---|---|
| Lena | Clustered-dot | Gaussian | - | - | - | - | 13.39 | 19.26 |
| | | LMS-S | 13.31 | - | - | - | 22.44 | 26.96 |
| | | LMS | 20.93 | 23.67 | 25.39 | 25.82 | 26.16 | 26.96 |
| | | MMSE | **22.41** | **25.31** | **26.14** | 23.96 | - | - |
| | | Hybrid | **22.41** | **25.31** | **26.14** | **26.96** | - | - |
| | Dispersed-dot | Gaussian | - | - | - | - | 26.44 | 28.30 |
| | | LMS-S | 23.69 | - | - | - | 28.15 | 28.31 |
| | | LMS | 24.81 | 26.15 | 27.04 | 27.85 | 28.17 | 28.31 |
| | | MMSE | **24.91** | 26.43 | 27.26 | 28.13 | - | - |
| | | Hybrid | **24.91** | **26.44** | **27.27** | **28.20** | - | - |
| | Error Diffusion | Gaussian | - | - | - | - | 26.82 | 30.41 |
| | | LMS-S | 24.36 | - | - | - | 31.40 | 32.39 |
| | | LMS | 24.61 | 28.21 | 30.03 | 31.59 | 32.16 | 32.39 |
| | | MMSE | **24.90** | **28.48** | 30.36 | 27.90 | - | - |
| | | Hybrid | **24.90** | **28.48** | **30.39** | **31.64** | - | - |
| Peppers | Clustered-dot | Gaussian | - | - | - | - | 13.64 | 19.52 |
| | | LMS-S | 13.50 | - | - | - | 22.53 | 27.26 |
| | | LMS | 20.82 | 23.66 | 25.41 | 25.94 | 26.34 | 27.26 |
| | | MMSE | **22.22** | 25.29 | 26.19 | 26.86 | - | - |
| | | Hybrid | **22.22** | **25.30** | **26.21** | **26.89** | - | - |
| | Dispersed-dot | Gaussian | - | - | - | - | 26.39 | 28.47 |
| | | LMS-S | 23.53 | - | - | - | 28.20 | 28.48 |
| | | LMS | 24.91 | 26.25 | 27.07 | 27.92 | 28.27 | 28.48 |
| | | MMSE | **25.21** | 26.59 | 27.35 | 28.04 | - | - |
| | | Hybrid | **25.21** | **26.60** | **27.39** | **28.26** | - | - |
| | Error Diffusion | Gaussian | - | - | - | - | 26.51 | 29.91 |
| | | LMS-S | 24.37 | - | - | - | 30.80 | 31.65 |
| | | LMS | 24.75 | 27.91 | 29.54 | 30.95 | 31.46 | 31.65 |
| | | MMSE | **25.11** | **28.39** | 30.09 | 28.00 | - | - |
| | | Hybrid | **25.11** | **28.39** | **30.13** | **31.23** | - | - |
| Lake | Clustered-dot | Gaussian | - | - | - | - | 14.22 | 19.64 |
| | | LMS-S | 14.10 | - | - | - | 21.27 | 24.49 |
| | | LMS | 19.76 | 22.41 | 23.57 | 23.82 | 24.02 | 24.49 |
| | | MMSE | **21.02** | 23.23 | **23.94** | **24.46** | - | - |
| | | Hybrid | **21.02** | **23.24** | **23.94** | **24.46** | - | - |
| | Dispersed-dot | Gaussian | - | - | - | - | 24.99 | 25.71 |
| | | LMS-S | 22.76 | - | - | - | 25.86 | 25.93 |
| | | LMS | **23.72** | 24.71 | 25.30 | 25.78 | 25.87 | 25.93 |
| | | MMSE | **23.72** | **24.89** | 25.44 | 25.93 | - | - |
| | | Hybrid | **23.72** | **24.89** | **25.45** | **25.96** | - | - |
| | Error Diffusion | Gaussian | - | - | - | - | 24.96 | 26.53 |
| | | LMS-S | 23.12 | - | - | - | 29.24 | 29.90 |
| | | LMS | 24.08 | 27.31 | 28.49 | 29.43 | 29.76 | 29.90 |
| | | MMSE | **24.30** | **27.42** | 28.54 | 24.38 | - | - |
| | | Hybrid | **24.30** | **27.42** | **28.68** | **29.31** | - | - |

7×7 Gaussian low-pass filter, $\sigma = 1.5$

5×5 Gaussian low-pass filter, $\sigma = 1.0$

TABLE II
NUMBER OF NONEMPTY CELLS AND EMPTY CELL FETCHES (IN PARENTHESES) OF THE MMSE METHOD WITH VARIOUS TABLE SIZES AND HALFTONE METHODS

| Image | Method \ Table Size | $2^9$=512 | $2^{13}$=8192 | $2^{16}$=65536 | $2^{21}$=2097152 |
|---|---|---|---|---|---|
| Lena | Clustered-dot | 500(0) | 3307(118) | 9064(358) | 26532(603) |
| | Dispersed-dot | 286(22) | 1494(119) | 3910(242) | 14225(577) |
| | Error Diffusion | 512(0) | 8174(2) | 60280(162) | 635739(11610) |
| Peppers | Clustered-dot | 500(1) | 3307(153) | 9064(504) | 26532(864) |
| | Dispersed-dot | 286(30) | 1494(176) | 3910(365) | 14225(922) |
| | Error Diffusion | 512(0) | 8174(3) | 60280(195) | 635739(10921) |
| Lake | Clustered-dot | 500(2) | 3307(231) | 9064(684) | 26532(1457) |
| | Dispersed-dot | 286(30) | 1494(150) | 3910(320) | 14225(891) |
| | Error Diffusion | 512(0) | 8174(9) | 60280(718) | 635739(25173) |

The initial filter mask is a square with the size of $L \times L$. In the experiments, however, the shape of the mask is not constrained to be square only, i.e., any shape is allowed. We use the LMS algorithm to perform the weight adaptation

$$w_{m+1}(k, l) = w_m(k, l) + 2\mu e(i-k, j-l)b(i-k, j-l) \quad \text{all } (k, l) \in M \tag{3}$$

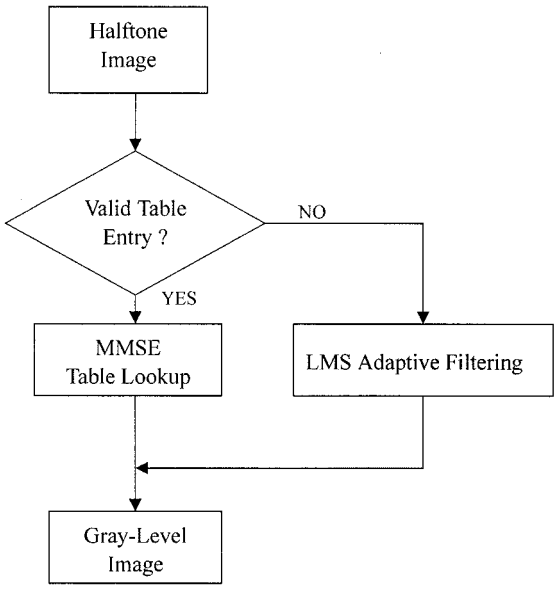


Fig. 5. Flowchart of the hybrid LMS-MMSE inverse halftoning method.

Fig. 6. Original grey-level image *Lena*.

where $m$ is the iteration index and $\mu$ is a parameter of updating step size that controls the stability and the rate of convergence. This iterative procedure terminates when the MSE decrease is negligible.

### B. Optimal Mask Shapes

In our experiments, 20 images with the size of $512 \times 512$ are used to train the reconstruction filter. The threshold matrices of ordered dither for the clustered-dot and dispersed-dot are $8 \times 8$ "Classical-4" and "Bayer-5," respectively [1]. The error diffusion uses a 12-order diffusion filter [2]. The image *Lena* is used to test the reconstruction filter. We start from a $7 \times 7$ square mask to reconstruct the gray-level pixel value of the central point.

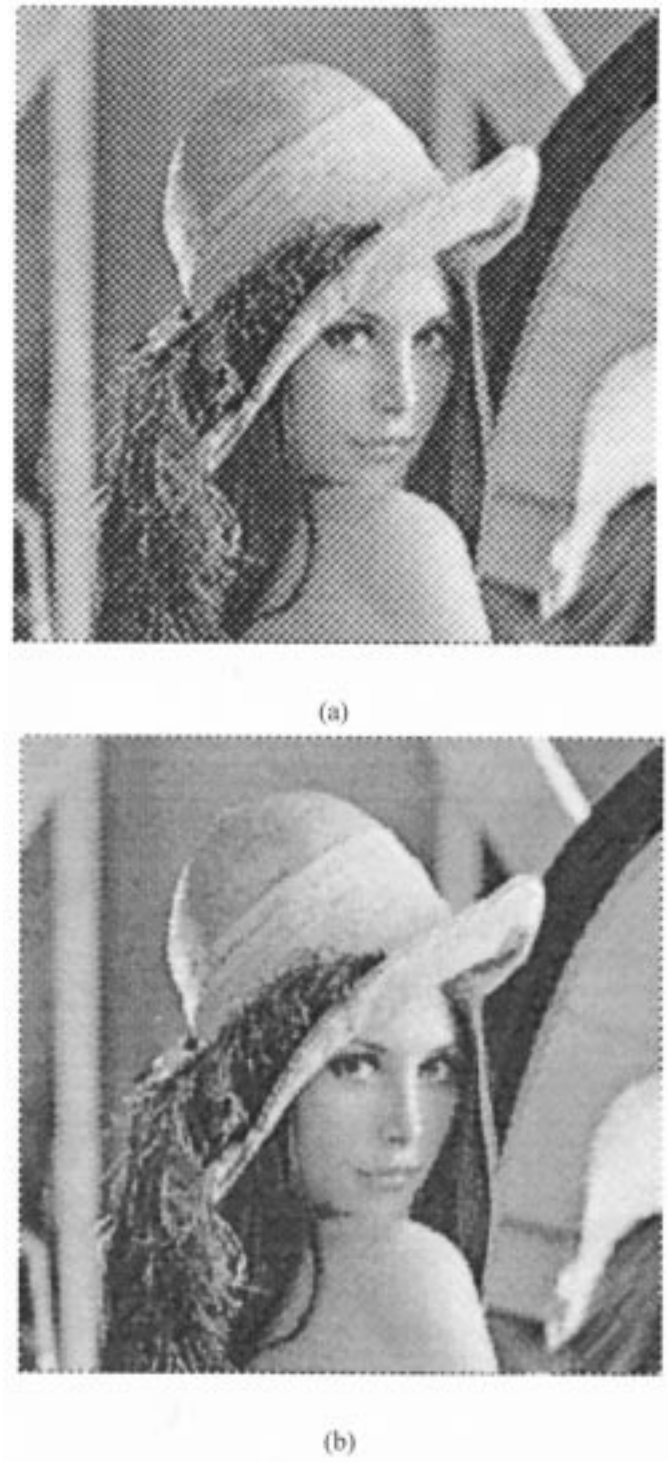


Fig. 7. Inverse halftoned *Lena* images from clustered-dot ordered dither: (a) $7 \times 7$ Gaussian filter, $\sigma = 1.5$ (19.26 dB) and (b) 21-point hybrid LMS-MMSE method (26.96 dB).

Then we eliminate the least significant weight that has the least absolute value and observe the mask shape as well as the variation of PSNR. The results for above three halftone methods are shown in Fig. 2. The pixels with light shade represent the shape of the mask. The pixel with a dark shade or "X" represents the center of the original mask, i.e., the pixel that the reconstructed value obtained from the filter output is placed. The center of the original mask does not necessarily exist in smaller masks. In this case, the center is marked by "X." The coefficients of the 16-point and 13-point filters for above three halftone methods are also listed in Fig. 3.

For clustered-dot ordered dither, the four corners of the mask are the first ones to be dropped. With 25 weights left, the mask shape is like a diamond and the PSNR is only 0.8 dB inferior to the 49-weight filter. With only 16 weights left, the mask boundary is still diamond, but some pixels including the central point in the diamond are dropped, and the filter mask becomes noncontiguous. From this observation, we learn that the significance of the filter weight is not necessarily inverse proportional to the distance to the mask center.

For dispersed-dot ordered dither, the four corners are still the first ones to be dropped. However, the mask is always contiguous no matter how low the filter order is. The PSNR is about 2 dB higher than that of clustered-dot at the same order. It is very interesting to notice that with limited order the optimal inverse halftoning mask for the clustered-dot is not clustered but dispersed, and vice versa. This conclusion seems not intuitive. However, a counter example may explain it. If we use a dispersed inverse halftoning mask for a dispersed-dot halftone image, then we may not get a smooth gray-level image. Instead, we get a near black value at one pixel and a near white value at next pixel. Hence, this should not be the optimal mask. Similarly, a clustered type inverse mask should not be the optimal mask for the clustered-dot halftoning.

For error diffusion halftone, bottom weights are generally dropped out earlier than top weights. When the order drops to nine, all surviving weights are on left and top sides only. This can be explained by the error diffusion halftoning process because errors are diffused to the right and bottom of the current pixel. Consequently, high correlation exists from top and left pixels in the error diffused halftone image. The PSNR is about 4 dB higher than that of dispersed-dot at the same order when the order is larger than 16 and the difference decreases when the order reduces. The optimal mask shapes obtained from the LMS algorithm will be applied to other inverse halftoning techniques in the rest of this paper.

## III. MMSE Table Lookup Inverse Halftoning

In this section, we present an optimal inverse halftoning method that minimizes the MSE between the reconstructed gray-level image and the original image. This minimum MSE (MMSE) method has an additional advantage that it is suitable for being implemented by table lookup. Thus, the computational complexity is greatly reduced.

### *A. Algorithm*

For a given mask with dimension $N$, the halftoning and inverse halftoning functions can be represented as the encoder and the decoder, respectively, of a sliding vector quantizer by ignoring the interblock correlation (or the sequential nature) of halftoning. The encoder maps a gray-level image to a binary halftoned image, i.e., it maps an $N$-dimensional Euclidean space to an $N$-dimensional binary space with up to the maximum number of $2^N$ codewords. From the vector quantization theory [22], the nearest neighboring mapping is optimal in the

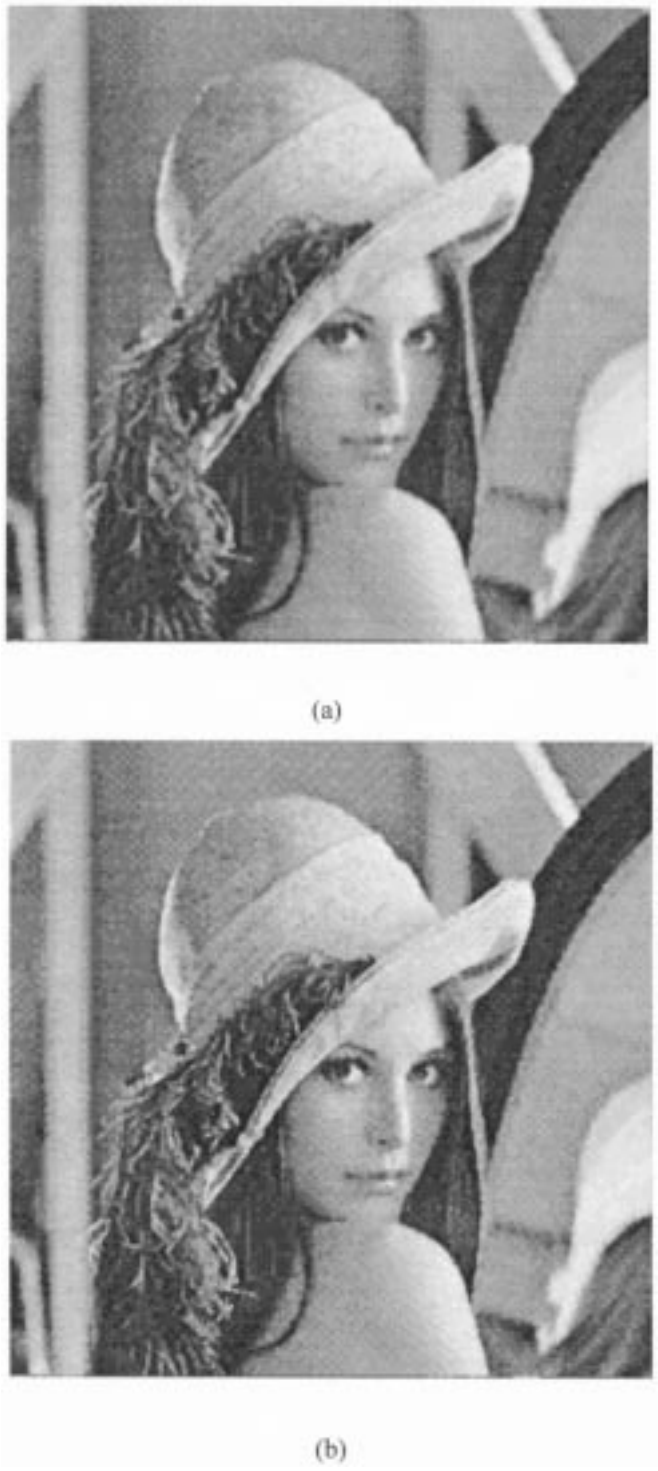

Fig. 8. Inverse halftoned *Lena* images from dispersed-dot ordered dither: (a) $7 \times 7$ Gaussian filter, $\sigma = 1.5$ (28.30 dB) and (b) 21-point hybrid LMS-MMSE method (28.20 dB).

sense of minimizing a distortion measure, such as the squared error. Any existing halftoning technique has its own mapping, which may be far from the optimal mapping. However, in this paper we only focus on the optimal inverse halftoning for the existing halftone methods.

The decoder maps an *N*-dimensional binary pattern to a one-dimensional Euclidean space. Specifically, it maps a bilevel block to a gray-level pixel that represents the reconstructed value of the central pixel in the mask. The optimal decoder for a given encoder is described by the centroid theorem [22] as follows.

*Centroid Theorem:* Given a nondegenerate partition $\{R_i\}$, the unique optimal codebook $\{Y_i\}$ for a random variable $X$ with respect to the mean square error is given by

$$Y_i = E[X|X \in R_i] \tag{4}$$

where

- $R_i$ set of the original gray-level pixels that are mapped to the $i$th binary halftone pattern;
- $X$ original gray-level pixel;
- $Y_i$ reconstructed gray-level pixel value with respect to the halftone pattern $i$.

In other words, the optimal inverse halftone codeword is the expected value of input pixels which are mapped to this codeword.

Because each halftone pattern is bilevel, there only exist at most $2^N$ halftone patterns for an $N$-dimensional mask. Thus, the inverse halftoning process is suitable for table lookup implementation due to the limited table size. The algorithm for the construction of the lookup table is described as follows.

*Step 1—Encoding Mapping:* Encode the gray-level images by a given halftone method. For a given $N$-point mask, keep tracking of the gray-level value of the central point in a mask and its corresponding halftone pattern. Record the histogram $T_i(a)$, i.e., the number of occurrences of the gray-level value *a* for each halftone pattern $i$.

*Step 2—Centroid Calculation:* For each halftone pattern $i$, calculate the centroid $Y_i$ of the central point of a mask. The centroid is calculated as the sample average

$$Y_i = \frac{\sum_{a=0}^{255} a \times T_i(a)}{\sum_{a=0}^{255} T_i(a)} \qquad i = 0, 1, \cdots, 2^N - 1. \tag{5}$$

*Step 3—Table Setup:* Fill in the centroids into a table with $2^N$ entries. This is the inverse halftoning reconstruction table. The reconstruction tables must be designed separately for different halftone methods for good performance.

### B. Experiments

The same sets of training and test images as in the last section are used in these experiments. The mask size affects the reproduction quality significantly. Fig. 4 illustrates an example. Fig. 4(a) first shows a nine-point halftone pattern and its corresponding histogram of gray-level pixel values for the clustered-dot ordered dither. The distribution of the gray-level values spreads over a wide range. It is obviously impossible to select a reconstruction value that can represent all the cases exactly. However, the patterns of the 13-point mask in Fig. 4(b) and (c) have much more concentrated distributions although they are classified as the same pattern with the nine-point mask. In general, large mask sizes are definitely able to generate good reproduction. The table size is, unfortunately, exponentially

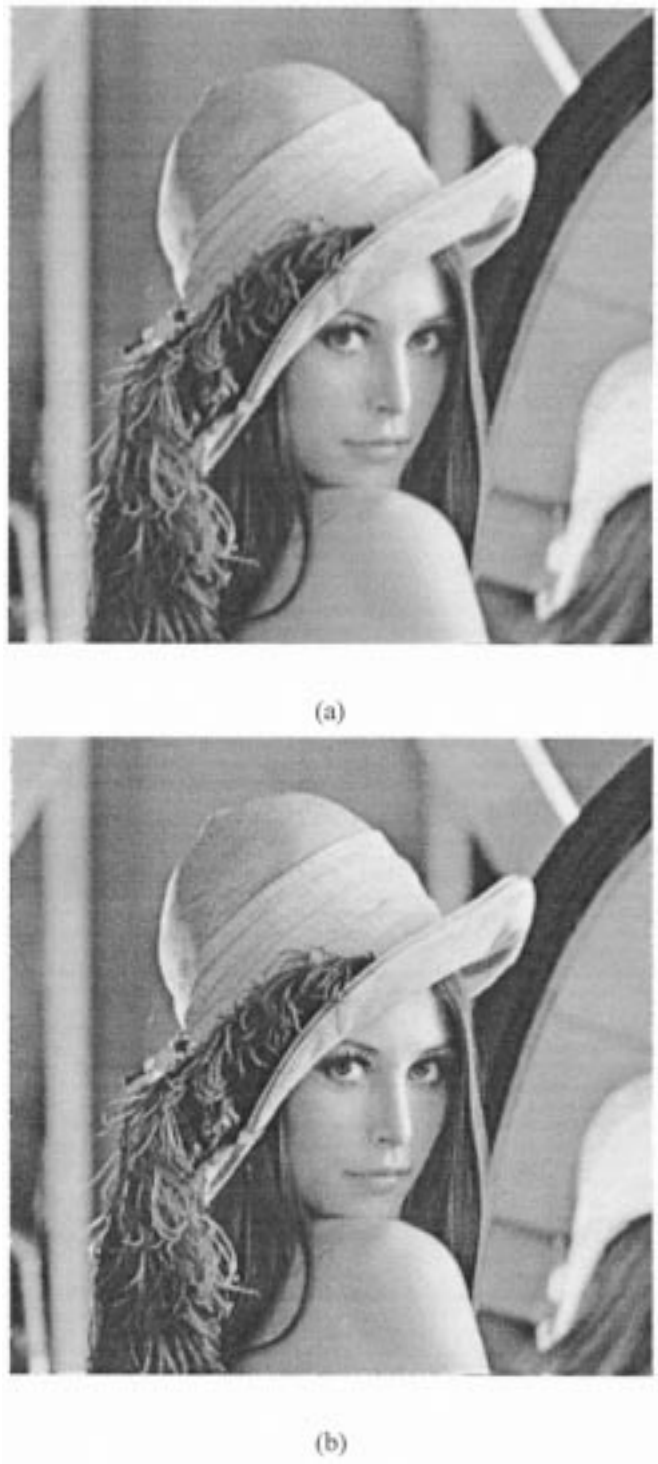

Fig. 9. Inverse halftoned *Lena* images from error diffusion: (a) $7 \times 7$ Gaussian filter, $\sigma = 1.5$ (30.41 dB) and (b) 21-point hybrid LMS-MMSE method (31.64 dB).

proportional to the mask size. For practical concerns, we use mask sizes no more than 21 points in experiments.

In addition to the mask size, the shape of the mask also affects the reproduction quality significantly. The optimal mask shapes developed by the LMS algorithm in the last section are applied. Three images (*Lena*, *Peppers*, and *Lake*) are used to evaluate the MMSE algorithm. Table I shows the reconstruction

TABLE III
COMPARISONS OF VARIOUS INVERSE HALFTONING METHODS FOR THE FLOYD–STEINBERG ERROR DIFFUSION KERNEL (IMAGE SIZE: $N \times N$ PIXELS, $N = 512$ HERE)

| Algorithm [Reference] | Memory Usage (Bytes) | Computational Complexity | PSNR (dB) | |
|---|---|---|---|---|
| | | | Lena | Peppers |
| POCS [8] | $8N^2$ | High | 30.4 | - |
| Bayesian [18] | $8N^2$ | High | - | - |
| Wong [9] | $8N^2$ | Medium | 31.00 | 29.30 |
| Wavelet [12] | $36N^2$ | Medium | 31.50 | 30.43 |
| Kite [17] | $7N$ | Low | 31.3 | 31.4 |
| Damera-Venkata [16] | $28N$ | Very Low | 31.51 | 31.17 |
| **16-point LMS-MMSE** | $\mathbf{2^{16}}$ | **Very Low** | **30.79** | **30.67** |
| **21-point LMS-MMSE** | $\mathbf{2^{21}}$ | **Very Low** | **31.39** | **31.22** |

quality, represented by PSNR, of the test images. The "LMS" and the "MMSE" columns represent the PSNR values of the LMS adaptive algorithm and the MMSE table lookup algorithm, respectively. The "Gaussian" and "LMS-S" columns also show the PSNR values reconstructed by the Gaussian and LMS square filters, respectively, for comparisons. In most cases, the MMSE method further improves the reconstruction quality for a given mask, which is generated from the LMS method. Particularly, the improvement for the clustered-dot ordered dither is significant. Among the three halftoning methods, the error diffusion still provides the best reconstruction quality.

Intuitively, the MMSE method should generate better reconstruction quality because it starts from the resultant optimal masks of the LMS method and in addition performs optimal mapping. However, the performance of the MMSE method is not necessarily better than the LMS method in all experiments. This seems to contradict the optimal decoding theorem of the vector quantization. In further investigation, we observe that the *empty cell* problem is serious in this table lookup implementation, particularly for the cases of large table sizes. An empty cell is defined as the halftone pattern or the table entry in which the number of input training samples mapping to it is less than or equal to a threshold. It happens when the training set is not sufficiently large or the halftone patterns generated by a halftone method only form a subset of $2^N$ binary space.

Table II shows the number of nonempty cells with the empty cell threshold set to zero in the training phase and the number of empty cell fetches, which represents the number of halftone patterns mapping to empty cells in the test phase. A larger set of training images should reduce the number of empty cells. Nevertheless, some halftone techniques, such as the ordered dithering methods, tend to use only a small subset of all possible patterns. This may explain why ordered dithering does not generate the best quality among all halftone methods. However, the limited use of the coding space has an advantage that only small table size is required if a proper hashing function is applied. On the other hand, the error diffusion technique tends to use as many patterns as possible. Hence, it has the potential to generate the best reconstruction quality.

In summary, the MMSE inverse halftoning technique has the optimal performance for a given mask and a halftone method provided that no empty cell fetches exist. This method is suitable for table lookup implementation. Intuitively, a sufficiently large set of training images can eliminate the empty cell problem. Unfortunately, due to the specific patterns of threshold matrices

or diffusion filters in these halftone methods, the empty cell problem still exists even with a relatively large set of training images. Therefore, we use the hybrid method as described in the next section to solve this problem.

## IV. Hybrid LMS-MMSE Inverse Halftoning

### A. Algorithm

We propose a hybrid inverse halftoning method that combines the LMS and the MMSE table lookup methods. The flowchart of this hybrid inverse halftoning method is shown in Fig. 5. The MMSE inverse halftoning method with the table lookup implementation has the advantages of good performance and fast processing speed. However, the empty cell problem degrades the performance. On the other hand, the LMS method never has this problem. Thus, the MMSE method is applied whenever the table entry is valid, and the LMS method is used as a complement to the MMSE method. Namely, for those halftone patterns with no corresponding table entries, the reconstructed gray-level value is determined by the filter that is designed by the LMS adaptive algorithm. The complete design procedure of the hybrid method is described as follows:

1) determine the maximum order of the LMS adaptive filter: $N$;
2) determine the maximum order of the MMSE method: $M$;
3) determine the optimal mask shapes by running the LMS adaptive filtering from $N$ points to $M$ points by dropping points with the smallest weights;
4) build up the reconstruction table by running the $M$-point MMSE design algorithm;
5) determine the empty cell threshold: $K$;
6) replace the empty cell table entry by the output of the $M$-point LMS adaptive filter for the same halftone pattern.

### B. Experiments

The same test images as in the previous sections are used in the experiments. The experiment results are also shown in Table I. The "hybrid" columns represent the PSNR values of the hybrid LMS-MMSE algorithm. The numbers in bold face are the best values among all five inverse halftoning methods. In all cases, the hybrid method is superior or equal to any of the LMS or MMSE methods. The empty cell threshold $K$ in the hybrid method is chosen to be 20 here. The value of $K$ affects the percentage that the MMSE method is used. The higher the $K$ is, the less likely the MMSE method is chosen. Although the MMSE method is optimal theoretically, a cell with very few samples may not provide good representation. Thus, the MMSE method with a small $K$ is not necessarily the best choice.

Fig. 6 shows the original gray-level test image of *Lena*. The photos of the reconstructed images by the Gaussian low-pass filter and the hybrid LMS-MMSE inverse halftoning method for three halftone techniques are demonstrated in Figs. 7–9. In particular, the proposed method has significant improvements over the Gaussian filter for the clustered-dot ordered dither and the error diffusion halftones. The hybrid LMS-MMSE approach reconstructed from the error diffused halftone still results in the best image quality, both objectively and subjectively.

Finally, we compare the image quality, memory usage, and computational complexity of the proposed hybrid method with various existing inverse halftoning methods for the Floyd–Steinberg error diffusion kernel [1]. The results are shown in Table III in which the memory usage and computational complexity of the existing methods are quoted from [16] and [17]. We observe that the 21-point hybrid LMS-MMSE method yields the comparable PSNR performance to the best results in all existing approaches. The computational complexity of the proposed method is extremely low in which only table lookup operations are involved. Although the memory usage is relatively high, it will not further grow up with the increase of the image size like all the other methods.

## V. Conclusion

We have presented the hybrid LMS-MMSE inverse halftoning method. The LMS adaptive algorithm is an efficient tool to discover the optimal filter masks. We obtain optimal filter masks for the three most commonly used halftone techniques. Based on these mask shapes, the MMSE table lookup method further improves the reconstruction performance and reduces the computational complexity. Finally, the hybrid method, which solves the empty cell problem, provides the best performance with a high processing speed. In particular, the proposed method is developed for existing halftoning techniques. The overall performance may be further improved if both the halftoning and inverse halftoning processes are optimized for each other.

## Acknowledgment

The authors would like to thank Dr. J. T. Wang, Dr. B. S. Jeng, and Dr. T. S. Liu of Chung-Hua Telecommunication Labs for their constant encouragement and discussions.

## References

[1] R. Ulichney, *Digital Halftoning*. Cambridge, MA: MIT Press, 1987.
[2] J. F. Jarvis, C. N. Judice, and W. H. Ninke, "A survey of techniques for the display of continuous-tone pictures on bilevel displays," *Comput. Graph. Image Process.*, vol. 5, pp. 13–40, 1976.
[3] M. Y. Ting and E. A. Riskin, "Error-diffused image compression using a binary-to-gray-scale decoder and predictive pruned tree-structured vector quantization," *IEEE Trans. Image Processing*, vol. 3, pp. 854–858, Nov. 1994.
[4] P. C. Chang and C. S. Yu, "Neural net classification and LMS reconstruction to halftone images," in *Proc. SPIE Conf. Visual Communications Image Processing*, vol. 3309, San Jose, CA, Jan. 1998, pp. 592–602.
[5] J. P. Allebach, "Reconstruction of continuous-tone from halftone by projections onto convex sets," in *Proc. Int. Conf. Advances Communication Control Systems*, Baton Rouge, LA, Oct. 19–21, 1988, pp. 469–478.
[6] M. Analoui and J. P. Allebach, "New results on reconstruction of continuous-tone from halftone," in *Proc. Int. Conf. Acoustics, Speech, Signal Processing*, San Francisco, CA, Mar. 23–26, 1992, pp. 313–316.
[7] Z. Fan, "Retrieval of gray images from digital halftones," in *Proc. Int. Symp. Circuits Systems*, May 1992, pp. 2477–2480.
[8] S. Hein and A. Zakhor, "Halftone to continuous-tone conversion of error-diffusion coded images," *IEEE Trans. Image Processing*, vol. 4, pp. 208–216, Feb. 1995.
[9] P. W. Wong, "Inverse halftoning and kernel estimation for error diffusion," *IEEE Trans. Image Processing*, vol. 4, pp. 486–498, Apr. 1995.
[10] Y. Mita, S. Sugiura, and Y. Shimomura, "High quality multi-level image restoration from bi-level image," in *Proc. Int. Congr. Advances Non-Impact Printing Technologies Black-and-White Color*, Orlando, FL, Oct. 21–26, 1990, pp. 791–802.

[11] J. Z. C. Lai and J. Y. Yen, "Inverse error-diffusion using classified vector quantization," *IEEE Trans. Image Processing*, vol. 7, pp. 1753–1758, Dec. 1998.
[12] Z. Xiong, M. T. Orchard, and K. Ramchandran, "Inverse halftoning using wavelets," in *Proc. IEEE Int. Conf. Image Processing*, vol. 1, Lausanne, Switzerland, Sep. 16–19, 1996, pp. 569–572.
[13] Y. T. Kim, G. R. Arce, and N. Grabowski, "Inverse halftoning using binary permutation filters," *IEEE Trans. Image Processing*, vol. 4, pp. 1296–1311, Sept. 1995.
[14] C. M. Miceli and K. J. Parker, "Inverse halftoning," *J. Electron. Imag.*, vol. 1, pp. 143–151, Apr. 1992.
[15] R. S. Kern, T. G. Stockham Jr., and D. C. Strong, "Descreening via linear filtering and iterative techniques," in *Proc. SPIE Conf. Human Vision, Visual Processing, Digital Display IV*, vol. 1913, San Jose, CA, Feb. 1993, pp. 299–309.
[16] N. Damera-Venkata, T. D. Kite, M. Venkataraman, and B. L. Evans, "Fast blind inverse halftoning," in *Proc. IEEE Int. Conf. Image Processing*, vol. 2, Chicago, IL, Oct. 4–7, 1998, pp. 64–68.
[17] T. D. Kite, N. Damera-Venkata, B. L. Evans, and A. C. Bovik, "A high quality, fast inverse halftoning algorithm for error diffused halftones," in *Proc. IEEE Int. Conf. Image Processing*, vol. 2, Chicago, IL, Oct. 4–7, 1998, pp. 59–63.
[18] S. M. Schweizer and R. L. Stevenson, "A Bayesian approach to inverse halftoning," in *Proc. SPIE Conf. Human Vision, Visual Processing, Digital Display IV*, vol. 1913, San Jose, CA, Feb. 1993, pp. 282–292.
[19] R. L. Stevenson, "Inverse halftoning via MAP estimation," *IEEE Trans. Image Processing*, vol. 6, pp. 574–583, Apr. 1997.
[20] B. Widrow and S. D. Stern, *Adaptive Signal Processing*. Englewood Cliffs, NJ: Prentice-Hall, 1985.
[21] L. M. Chen and H. M. Hang, "An adaptive inverse halftoning algorithm," *IEEE Trans. Image Processing*, vol. 6, pp. 1202–1209, Aug. 1997.
[22] A. Gersho and R. M. Gray, *Vector Quantization and Signal Compression*. Norwell, MA: Kluwer, 1992.

**Pao-Chi Chang** was born in Taipei, Taiwan, R.O.C., in 1955. He received the B.S. and M.S. degrees from National Chiao Tung University, Hsinchu, Taiwan, in 1977 and 1979, respectively, and the Ph.D. degree from Stanford University, Stanford, CA, in 1986, all in electrical engineering.

From 1986 to 1993, he was a Research Staff Member with the Department of Communications, IBM T. J. Watson Research Center, Hawthorne, NY, where his work centered on high-speed switching system, efficient network design algorithms, network management, and multimedia teleconferencing. In 1993, he joined the faculty of National Central University, Chung-Li, Taiwan. His current interests are in the area of speech/image coding, video conferencing, and video coding over high-speed networks and wireless communications.

**Che-Sheng Yu** was born in Taipei, Taiwan, R.O.C., in 1970. He received the B.S. and M.S. degrees in electrical engineering from National Central University (NCU), Chung-Li, Taiwan, in 1992 and 1997, respectively.

From 1994 to 1995, he was a Teaching Assistant with the Electrical Engineering Department, NCU. His research interests include digital image/video processing, neural network, and ASIC design. Currently, he is an IC Design Engineer with the R&D Department, Sunplus Technology Co., Ltd., Taiwan, where he contributes to the hardware design for multimedia devices.

**Tien-Hsu Lee** was born in Hsinchu, Taiwan, R.O.C., in 1971. He received the B.S. degree in 1993 from National Cheng Kung University, Taiwan, and the Ph.D. degree in 2000 from National Central University, Chung-Li, Taiwan, both in electrical engineering.

His current interests are in the area of image/video coding, error prevention and concealment techniques, and wireless network applications.